Journal of Power Sources 218 (2012) 261–267

Contents lists available at SciVerse ScienceDirect

Journal of Power Sources

journal homepage: www.elsevier.com/locate/jpowsour

Effects of interlayer thickness on the electrochemical and mechanical properties of bi-layer cathodes for solid oxide fuel cells

Qing Su [a], Daeil Yoon [b], Young Nam Kim [b], Wenquan Gong [c], Aiping Chen [d], Sungmee Cho [d], Arumugam Manthiram [b], Allan J. Jacobson [c], Haiyan Wang [a,d,*]

[a] Material Science and Engineering Program, Texas A&M University, College Station, TX 77843-3003, USA
[b] Electrochemical Energy Laboratory & Materials Science and Engineering Program, University of Texas at Austin, Austin, TX 78712, USA
[c] Department of Chemistry, University of Houston, Houston, TX 77204-5003, USA
[d] Department of Electrical and Computer Engineering, Texas A&M University, College Station, TX 77843-3128, USA

HIGHLIGHTS

- Nanoporous LSCO interlayers grown by pulsed laser deposition.
- The interlayer thicknesses varied from ~50 nm to ~500 nm.
- Improved electrochemical and mechanical properties of the bi-layer cathodes observed.
- Significantly improved cell performance demonstrated with bi-layer cathode.

ARTICLE INFO

Article history:
Received 15 May 2012
Received in revised form
26 June 2012
Accepted 28 June 2012
Available online 5 July 2012

Keywords:
Bi-layer cathode
$La_{0.5}Sr_{0.5}CoO_{3-\delta}$
Thin film SOFC
Thickness variation
Hybrid method

ABSTRACT

A hybrid method that combines an interlayer prepared by a pulsed laser deposition (PLD) technique and a conventional cathode prepared by a screen printing method is employed to fabricate bi-layer $La_{0.5}Sr_{0.5}CoO_{3-\delta}$ (LSCO) cathodes. Robust bi-layer cathode films are successfully fabricated with a porous microstructure and excellent integrity with the underlying electrolyte layer. By adjusting the thickness of the PLD interlayers from ~50 to ~500 nm, a systematic variation of the electrochemical and mechanical properties of the bi-layer cathodes is observed. Compared with single cells without an interlayer, the anode-supported single cells with an LSCO interlayer thickness of ~100 nm exhibit significant enhancement in the overall power performance.

1. Introduction

Because of their efficient and clean energy production, solid oxide fuel cells (SOFCs) have attracted extensive research interest [1–4]. Compared with bulk SOFCs, thin film SOFCs (TFSOFCs) are more cost-effective, have wider range of fuel options and higher fuel efficiency, and are considered to be one of the possible energy harvesting alternatives [5,6]. Recent research efforts mainly focus on lowering the TFSOFCs operating temperature (500–700 °C or lower) by exploring new materials and optimizing the component microstructures. Research has also focused on enhancing the long-term stability of THSOFCs [7–9]. The cathode and cathode/electrolyte interface, where oxygen reduction and transport take place, are believed to play a significant role on the overall SOFC performance and have, therefore, attracted ongoing research efforts [10,11].

Screen printing, a low cost simple process, is one of the most conventional and widely used fabrication methods to prepare cathode layers with thickness ≥ 10 μm [12]. The high-temperature thermal treatment (over 1100 °C), which is required after the screen printing process to ensure the adhesion between the cathode and the electrolyte can, however, cause serious shrinkage in the film thickness, leading to cracks and possible delamination [8,9]. This has raised concerns about the reproducibility and reliability of cathode layers prepared by screen printing. In contrast to screen printing, pulsed laser deposition (PLD) can be used to prepare thinner films with thicknesses from tens to hundreds of

* Corresponding author. Department of Electrical and Computer Engineering, Texas A&M University, College Station, TX 77843-3128, USA. Tel.: +1 979 845 5082.
E-mail address: wangh@ece.tamu.edu (H. Wang).

0378-7753/$ – see front matter © 2012 Elsevier B.V. All rights reserved.
http://dx.doi.org/10.1016/j.jpowsour.2012.06.094

nanometers. PLD can be used to fabricate cathode thin films with well-controlled microstructure by adjusting the deposition parameters [13,14], but the cost is higher due to the low growth rate and high processing cost. For example, to grow a 5–6 μm thick cathode, it may take 2–4 h of PLD deposition depending on materials and laser energy (the estimation is based on the growth rate of 0.5–1 Å pulse^{-1} and the pulse rate of 5–10 Hz). The hybrid method reduces the cost significantly compared with the PLD only method. In our previous work, PLD was used to grow the interlayer with nanopororous microstructure followed by a thick cathode layer (~7 μm) prepared by the screen printing method [11]. The hybrid method was shown to combine the advantages of both techniques, namely the cost effectiveness of screen printing and the well-controlled microstructure provided by PLD for the preparation of thick cathode films with well controlled pore structures. A 500 nm thick PLD interlayer was used for the preliminary demonstration.

The interlayer approach has been applied in SOFCs to enhance performance and stability. For example, a composite LSCO–$Ce_{0.9}Gd_{0.1}O_{1.95}$ (CGO) interlayer between electrolyte and cathode has been used as a catalytic layer or transition layer to mitigate thermal stress and lattice strain at the interface [14]. Also, inserting an yttria-doped ceria (YDC) interlayer between the bulk electrolyte and the cathode has been demonstrated to enhance the performance of low-temperature solid oxide fuel cells. The interlayer helps to lower the reaction barrier and to enhance the catalytic reaction probability [15]. In the hybrid approach, the interlayer prepared by the PLD method with a nanoporous structure could provide channels for oxygen gas transport and increase the effective contact area at the gas–cathode–electrolyte triple phase boundaries (TPBs). Also, it provides more nucleation sites for the screen printing layer, consequently producing excellent adhesion between the electrode and the electrolyte as well as a formation of uniform pores in cathode film. Because the interlayer is made of nanoporous LSCO, which is a mixed conducting cathode material [16], it is expected that the interlayer thickness is closely related to the number of reaction sites, the reaction and diffusion rate of oxygen, and the microstructure of the electrodes. However, up-to-date, no detailed study of the effect of thickness variation of the interlayer on the cathode performance and reliability has been made. In this paper, PLD interlayers with different thicknesses are applied between the screen printed cathode and the electrolyte layer to prepare a set of TFSOFCs. The mechanical and electrochemical properties of those hybrid cathodes are examined and correlated with the microstructure to probe the effect of interlayer thickness. Some guidelines for designing high-performance bi-layer cathodes with optimum performance and low cost are proposed.

2. Experimental

2.1. LSCO powder and PLD target processing

The PLD targets including LSCO, 8 mol% yttria stabilized zirconia (YSZ) (500 nm, Tosoh Co.), $Ce_{0.9}Gd_{0.1}O_{1.95}$ (CGO), 60 wt.% NiO + 40 wt.% YSZ (NiO–YSZ, 500 nm, Praxair Inc.), and CGO electrolyte disks were all fabricated by solid-state reaction through mixing stoichiometric amounts of the raw powders: La_2O_3 (99.99%), $SrCO_3$, Co_3O_4 (99.9%), CeO_2 (99.9%), and Gd_2O_3 (99.9%). The sintering details can be found elsewhere [14]. The phase purity of LSCO, CGO, and YSZ were confirmed by X-ray diffraction (XRD). The LSCO powders for the preparation of screen printing slurry were obtained from the LSCO target with a pseudo-cubic structure. The LSCO target was crushed into powders and then the powders were ball milled for 30 h to refine the particle size. The surface area of those powders was 3.2 g m^{-2} measured by Brunauer-Emmett-Teller (BET) surface adsorption method.

2.2. Symmetric cells and single cells fabrication

The LSCO interlayers with different thicknesses were deposited on pressed sintered $Ce_{0.9}Gd_{0.1}O_{1.95}$ (CGO) disks in a PLD system with a KrF excimer laser (Lambda Physik Compex Pro 205, $\lambda = 248$ nm). The laser beam with approximately 5 J cm^{-2} in energy density was focused on the targets at a 45° incident angle. The thicknesses of the PLD interlayer were controlled from ~50 to ~500 nm by deposition time to optimize the microstructure of the PLD interlayer and the subsequent screen printed layer. In order to fabricate the symmetric cells for impedance measurement, the LSCO slurry was screen printed onto CGO substrates coated with PLD interlayer of different thicknesses. The cells were then annealed at 1150 °C for 2 h with a ramping rate of 2 °C min^{-1}. To prepare the single cells, commercial NiO–YSZ cermet powder was compacted into anode disks under uniaxial pressure using an 1 inch (2.54 cm) diameter die set. The disks were then sintered at 1300 °C for 3 h. Subsequently, a bi-layer electrolyte (1.5 μm YSZ deposited prior to a 6 μm CGO layer), a PLD LSCO thin-film cathode layer, and a screen printed LSCO cathode layer were deposited onto a NiO–YSZ anode disk substrate under the conditions described in our previous work [14,17].

2.3. Microstructure and mechanical characterizations of symmetric cells

The microstructure of these films was first characterized by a high resolution field emission scanning electron microscope (FE-SEM, JEM-7500F Cold Emission SEM) and a transmission electron microscope (TEM, JEOL 2010). The hardness of the cathode films was measured by a commercial Fischerscope HM2000XYp micro-indentation with Vickers indenter. The film was indented down to 500 nm and a minimum of twenty indents were performed on each specimen to obtain the average hardness value.

2.4. ASR of symmetric cells and power density measurements of single cells

Platinum grids were gently pressed onto porous electrodes and were used as current collectors. Using a potentiostat/impedance analyzer (Reference 600™, Potentionstat/Galvanstat/ZRA, GAMRY INSTRUMENTS), AC impedance spectroscopy measurements were conducted in the frequency range of 10^{-2}–3×10^5 Hz in the temperature range from 400 to 700 °C. The AC impedance data were measured after a waiting period of an hour for temperature stabilization. The anode-supported single cells prepared with and without interlayer were used to evaluate the interlayer effect on the cathode performance. Humidified H_2 with a constant flow rate of 80 mL min^{-1} and air with at a constant flow rate of 120 mL min^{-1} were supplied as the fuel and the oxidant, respectively, during the single-cell performance test. Measurement details can be found elsewhere [14,17].

3. Results and discussion

The X-ray diffraction (XRD) patterns of the LSCO cathode film with and without the PLD interlayer on CGO pellet are shown in Fig. 1. The symbol * refers to LSCO peak and the symbol # refers to CGO peak. The diffraction peaks of LSCO match well with the standard PDF card (#048-0122), which indicates a pure poly-crystalline LSCO phase with a pseudo-cubic structure [18]. There is no obvious variation in the crystal structure between the LSCO cathodes with and without the PLD LSCO interlayer.

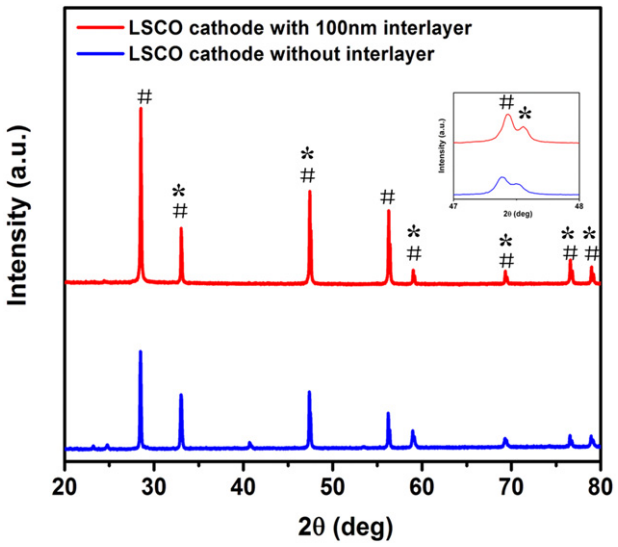

Fig. 1. The X-ray diffraction (XRD) patterns of the LSCO cathode film with and without the PLD interlayer. The inset shows a magnification of XRD peaks around 47.5°. The symbol * refers to LSCO peak and the symbol # refers to CGO peak.

To examine the interlayer effect on the microstructure of the LSCO cathode films, the cathode films with and without the PLD interlayer were characterized by cross-section SEM, as shown in Fig. 2a–d. Fig. 2a and b show that LSCO particles agglomerated into big and dense grains when there is no PLD interlayer (Fig. 2a) or when the PLD interlayer is very thin (<50 nm, Fig. 2b). Compared with the screen-printed only films and the bi-layer cathode films with a very thin PLD interlayer, the LSCO films prepared with thick PLD interlayer as seen in Fig. 2c (106 nm), and d (530 nm) show much smaller grains with uniform pores and good grain connectivity between the electrolyte and cathode films. The PLD interlayer thickness apparently plays an important role in the nucleation process of the screen printed layer.

To further confirm the interlayer effect on the screen printed layer, the screen printed cathodes without and with a PLD interlayer were characterized by plan-view SEM and shown in Fig. 3a and b, respectively. It is clear that the sample with PLD interlayer shows the enhanced surface coverage and smaller grains indicating that the nano-porous PLD interlayer could greatly increase the nucleation sites for the following screen-printed layer leading to uniform grain size and porous structure after sintering process. This is further supported by the cross-section TEM (XTEM) study in Fig. 3c, where a good grain connectivity between the PLD interlayer and the porous screen printed LSCO layer is clearly observed.

To measure the electrochemical performance of the LSCO cathodes with different PLD interlayer thicknesses and the samples without PLD interlayer, symmetric cells with different PLD LSCO interlayer thicknesses were prepared. The PLD LSCO interlayer thickness was controlled through the deposition time. A relatively high temperature (1150 °C) was used for all the samples because it is the optimized temperature for sintering the screen printed cathode film. To ensure a fair comparison between the single layer and bi-layer cathodes, the same sintering temperature for all samples was used. However it was found that the sintering temperature of the bi-layer cathode could be as low as 800 °C and there is still good grain connectivity between the screen-printed layer and the PLD interlayer and comparable electrochemical performance as those sintered at 1150 °C. This is another advantage for incorporating a thin PLD interlayer. The specific impedance data of symmetric cells with cathode prepared by screen printing only method and hybrid method with ~500 nm PLD interlayer at 600 °C are plotted in Fig. 4a. The low frequency semicircle in Nyquist plot

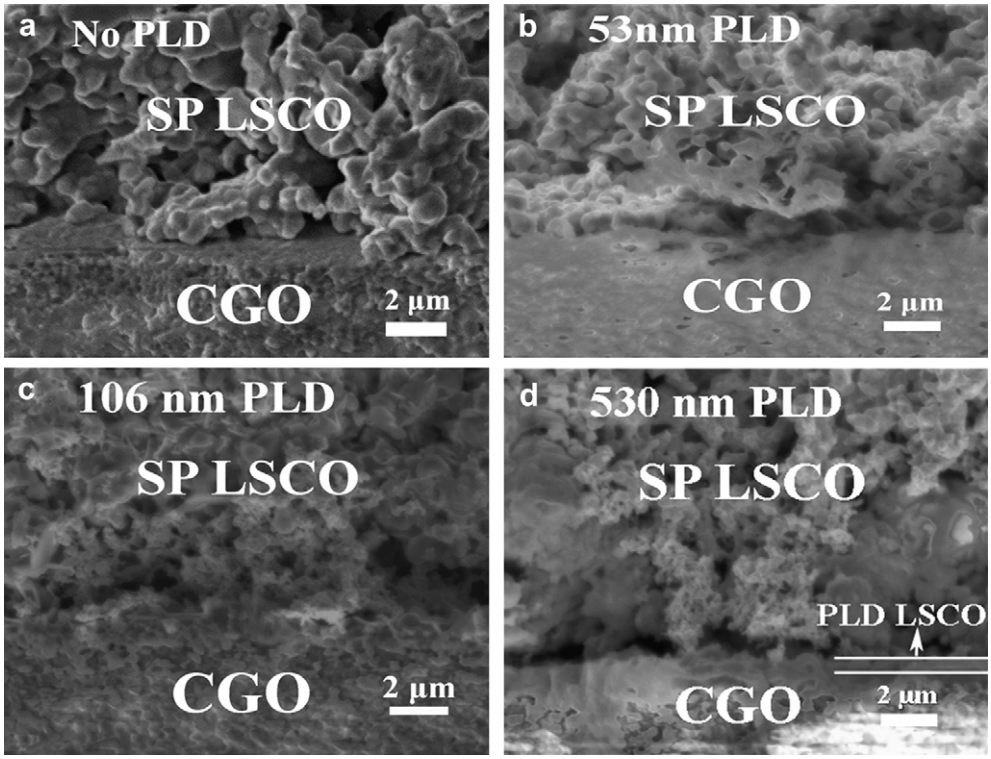

Fig. 2. Cross-section SEM images of screen printed LSCO layer (a) directly onto CGO pellet and onto PLD LSCO interlayer with different thicknesses of (b) 53 nm, (c) 106 nm, (d) 530 nm. All samples were annealed at 1150 °C for 2 h.

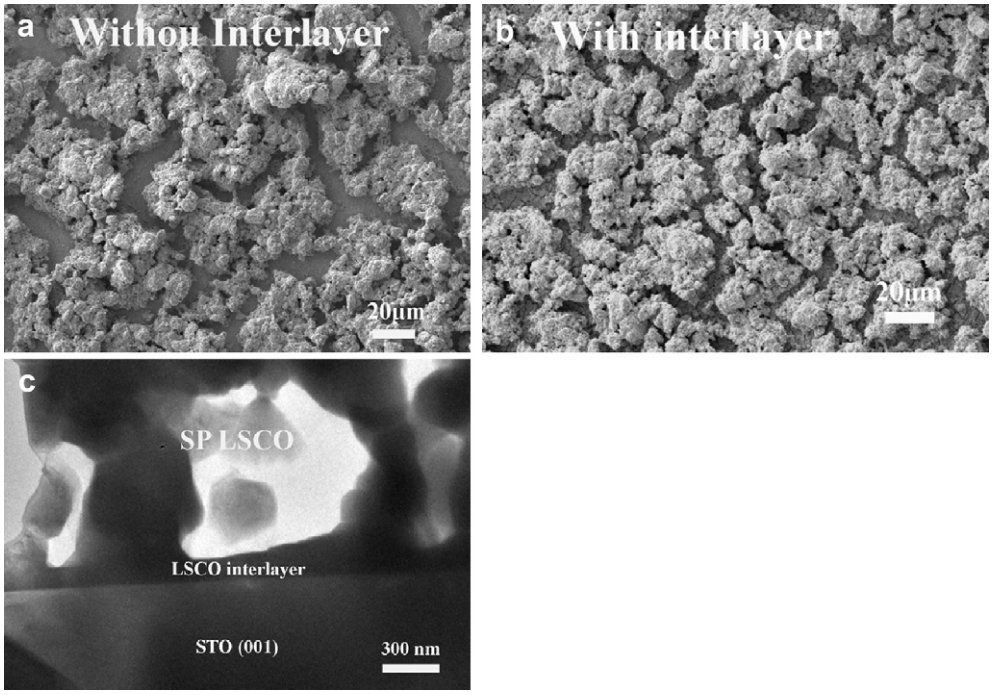

Fig. 3. Plan-view SEM images of screen printed cathode (a) without and (b) with PLD interlayer and (c) a cross-section TEM image of bi-layer cathode.

represents the polarization resistance [13]. There is a significant enhancement for the cathode prepared by the hybrid method compared to that prepared by the screen printing only method. The following equation was used to calculate the area specific resistance (ASR): ASR = R_p*A/2, where R_p is the electrode polarization resistance, which equals to the diameter of the low frequency semicircle and A is the geometric electrode area. An Arrhenius plot of ASR as a function of temperature for the cathode layers with different PLD interlayer thicknesses is plotted in Fig. 4b. The ASR of single layer LSCO cathode films prepared by conventional screen printing method and pulsed laser deposition are also plotted for comparison [11,19]. Previously the ASR of screen printed LSCO cathode was reported to be 2–4 Ω cm^2 at 600 °C, while the ASR of the PLD LSCO cathode was as low as 0.09 Ω cm^2 at 600 °C [11]. By comparison with ASR of the screen printed LSCO cathode, the ASR significantly decreases by inserting the PLD interlayer (Fig. 4b). The ASR of bi-layer cathode films decreases with increasing PLD interlayer thickness from ~50 to ~500 nm. A slight ASR decrease is observed with a PLD interlayer with the thickness of 53 nm. When the PLD interlayer thickness is ~100 nm, the ASR of bi-layer LSCO cathode drops to ~one fifth of those of the films prepared by the screen printing only method. The ASR seen as the inset in Fig. 4b, however, decreases only slightly for thicker PLD interlayers up to 530 nm. Since LSCO is a mixed electric-ionic conducting cathode material and the PLD interlayer plays the role of a catalytic layer, the decrease of ASR can be explained by the expanded oxygen

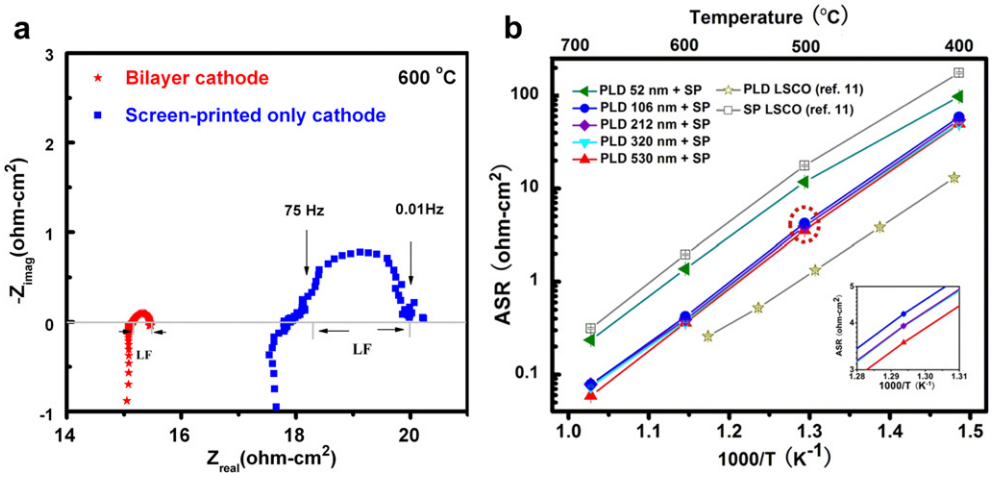

Fig. 4. (a) The specific impedance data of symmetric cells with cathode prepared by the screen printing only method and the hybrid method with 500 nm PLD interlayer at 600 °C and (b) the ASR of the symmetric cells with different PLD LSCO interlayer thickness and without PLD LSCO layer as a function of measurement temperature in air. The inset in (b) shows a magnified ASR plot of the symmetric cells with PLD LSCO interlayer thickness range from 106 nm to 530 nm at 600 °C.

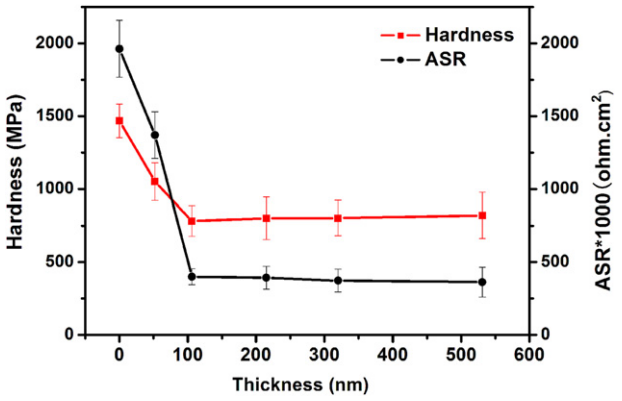

Fig. 5. The hardness and ASR at 600 °C of the symmetric cells as a function of the PLD LSCO interlayer thickness.

reduction reaction zone. It is expected that the interlayer thickness effect could be more significant for the cathode materials with higher ionic conductivity such as $Ba_{0.5}Sr_{0.5}Co_{0.8}Fe_{0.2}O_{3-\delta}$ (BSCF), $PrBaCo_2O_{5+\delta}$, $La_2NiO_{4+\delta}$, etc [20–22].

To further confirm the microstructure variation of those bi-layer cathode films with different PLD interlayer thicknesses, micro-indentation was conducted to test the hardness of those films. Because material hardness is inversely proportional to film porosity, hardness could be an indirect indicator of film porosity [23]. The error bar was estimated by taking into account both error from the hardness measurement and the data fitting. From Fig. 5, it is evident that the hardness has a sharp decrease as the PLD interlayer increases from 0 to 100 nm, which suggests the cathode films have a significant change in microstructure in this range. The sample without the PLD interlayer has mostly large grains (Fig. 2a) and shows a high hardness of ~2 GPa and high ASR of 2 Ω cm^2 at 600 °C. However the sample with the 100 nm PLD interlayer has much finer grains (Fig. 2c) and high porosity in the sample and, therefore, has a lower hardness of 0.5 GPa and lower ASR value. This again demonstrates that the PLD interlayer with a nanoporous microstructure provides more nucleation sites for the screen printed cathode layer. The hardness remains relatively constant when the PLD interlayer thickness is increased to ~500 nm, which suggests that the screen printed layers have similar porosity when the PLD layer is ≥ 100 nm thick. Considering that the electrolyte surface is not perfectly flat, the microstructure of the thin films in the first tens of nanometer thickness range could still be isolated islands, which do not cover the entire surface of the electrolyte substrate based on the thin film growth model [24,25]. Although it indeed provides more nucleation sites, the uncovered areas still have the screen printing particles agglomerated into large grains similar to the case of the screen printed only film. When the PLD interlayer thickness reaches 100 nm, it is expected that most of the electrolyte surface is covered by the PLD interlayer and, therefore, the microstructure of the screen printed layer shows much smaller grains with pores. The microstructure and hardness of the cathode layers remains the same for the samples with thicker PLD layers.

Based on the above results, schematics of the microstructures for LSCO cathode films with and without PLD LSCO interlayer are presented in Fig. 6a. The cathode film without PLD interlayer is consisted of scattered large grains on the uneven electrolyte surface and thus is low in film porosity. After inserting nano-porous PLD interlayers, the films show significantly enhanced surface coverage with uniform pores after high temperature sintering.

To demonstrate the PLD interlayer effect on the overall cell performance, the anode-supported single cells with and without PLD interlayers were prepared. The single cell with interlayer thickness of 100 nm was selected to ensure the enhancement with

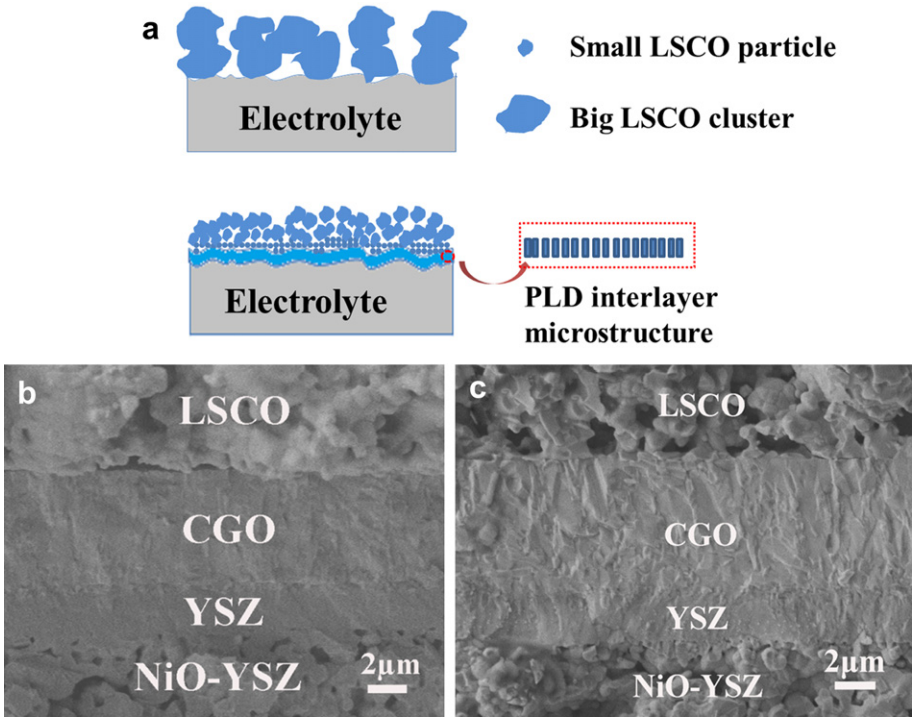

Fig. 6. (a) The proposed scheme of different microstructures and the different microstructures of single cells (b) without PLD LSCO interlayer and (c) with ~100 nm PLD LSCO interlayer.

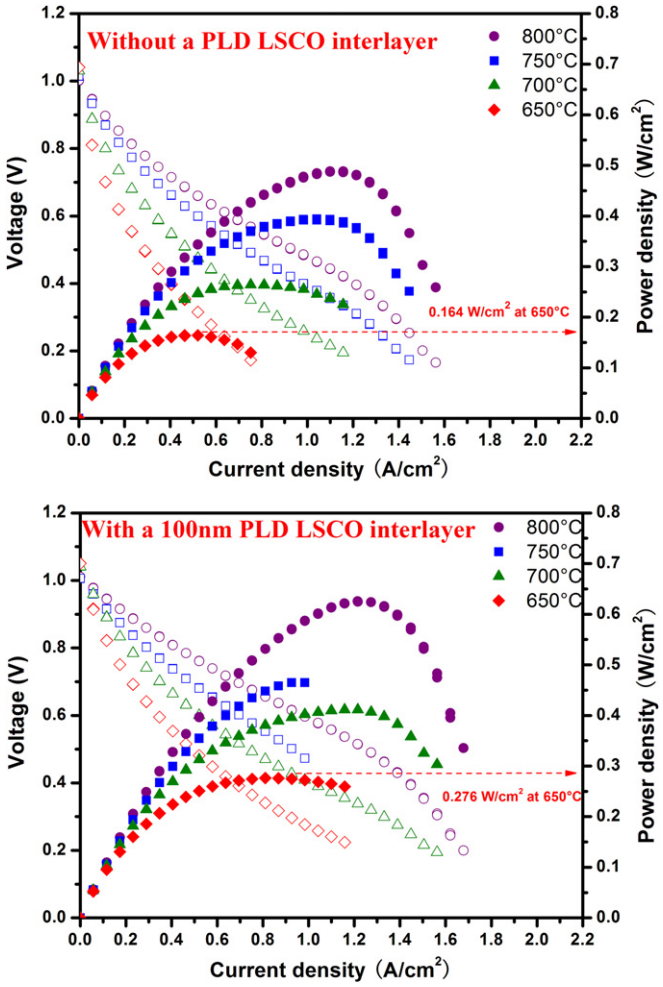

Fig. 7. The power density of single cells with and without PLD LSCO interlayer from 650 to 800 °C.

the minimal interlayer thickness. As seen from the cross-section SEM images of single cells with and without PLD interlayer, a dense and crack-free bi-layer electrolyte of YSZ (~1.5 μm) and CGO (~6.0 μm) was successfully prepared on the porous NiO–YSZ anode (Fig. 6b). A YSZ thin layer is applied to prevent the reduction of Ce^{4+} into Ce^{3+}, which occurs in hydrogen atmosphere and leads to a decrease in open circuit voltage (OCV) [26]. Compared with the dense and large grains shown in Fig. 6b, the cathode with much higher porosity, smaller grains, and better adhesion with the electrolyte was observed (Fig. 6c) for the cell with the 100 nm PLD interlayer.

The current–voltage (I–V) characteristics of the anode-supported single cells were measured by a two-electrode set-up. Pt wires were used as electrical contacts held by Pt paste. The performance was measured at the temperatures ranging from 650 to 800 °C. The cell voltage and power density as a function of current density for the sample without the PLD interlayer is shown in Fig. 7. The open circuit voltage (OCV) is 1.04 V at 650 °C, and the maximum power densities of the cell are 0.164 (highlighted with a red arrow), 0.264, 0.394, and 0.488 W cm^{-2} at 650, 700, 750, and 800 °C, respectively. The overall trend is that the power density decreases as the measurement temperature decreases, and the cell potential also decreases as a result of the increasing polarization losses across the cell with increasing current density. The cell with the PLD interlayer (Fig. 7) provides an OCV of 1.05 V at 650 °C and the maximum power densities of 0.276 (highlighted with red arrow), 0.412, 0.466, and 0.626 W cm^{-2}at 650, 700, 750, and 800 °C, respectively. Compared with the cell without an interlayer, the cells with the interlayer have more than 50% increase in the overall maximum power density at both 650 and 700 °C and ~30% increase in the power density at 800 °C.

The cross-section SEM images of the single cells with and without PLD interlayer are shown in Fig. 8a and b. It is clear that, after ~2–3 day power measurements, the single cells with PLD interlayer remains a sharp interface between the electrolyte and the cathode. However, for the sample without PLD interlayer, there is a small gap in several regions along the electrolyte/cathode interface. In addition, it has been previously reported that nano-porous interlayer could present much larger thermodynamic factor than some of the powder samples [13]. The larger thermodynamic factor will result in a smaller change in the composition at different temperatures for cathode films [13], i.e., a longer lifetime and better cyclability for the cells with bi-layer cathode. The study suggests that the interlayer approach could improve the surface adhesion between the electrolyte and the cathode layer, and thus lead to the long term durability of the cells.

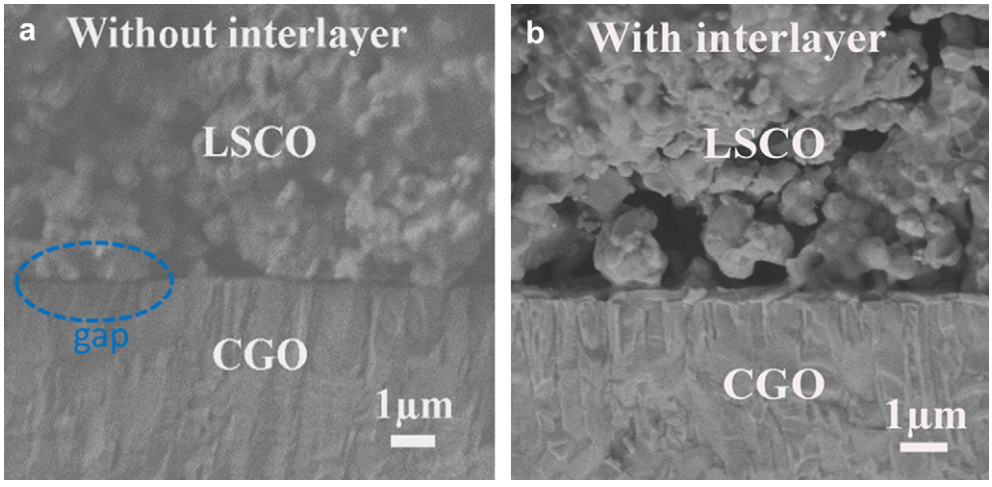

Fig. 8. The cross-section SEM images of single cells (a) without and (b) with the PLD interlayer after power density measurement.

4. Conclusions

Bi-layer cathodes with different PLD interlayer thicknesses have been successfully fabricated by combining PLD with the screen printing method. Compared with layers of screen printed LSCO directly onto aCGO electrolyte, the LSCO layers with a thin PLD interlayer (<50 nm) show moderate grain size and enhanced film porosity, while the LSCO layers with a thick PLD interlayer (thickness $\geq$ 100 nm) have much higher film porosity with small grains and uniform pore structures. The mechanical and electrochemical measurement results of those cathodes agree well with the microstructure analysis. There is a slight decrease in ASR and hardness if the applied interlayer thickness is thin (50 nm); while the ASR is about 5 times lower than that of the single layer cathode when the thickness is $\geq$ 100 nm and the film porosity and grain size reach their optimum level based on the hardness measurement. The anode-supported single cells with PLD interlayers demonstrated enhanced power performance at all temperatures compared with the cells without the interlayer. The maximum power densities of the single cells are 0.276, 0.412, 0.466, and 0.626 W cm^{-2} at 650, 700, 750, and 800 °C, respectively, with an OCV of 1.05 V at 650 °C. There is a 50% enhancement in power density in the temperature range from 650 to 700 °C and ~30% increase at 800 °C. Overall, the results strongly support that the thin PLD interlayer improves the electrochemical performance of the cathode layer as well as the overall cell performance and cell integrity.

Acknowledgments

The work was supported by the National Science Foundation (NSF-0846504 and NSF 1007969). D.Y, Y.N.K, and A.M acknowledge the support from the Robert A. Welch Foundation (Grant No. F-1254). A.J.J and W.G acknowledge the support from the Robert A. Welch Foundation (Grant No. E-0024) and the U.S. Department of Energy (U.S. DOE), Office of Basic Energy Sciences, Division of Materials Sciences and Engineering (under Award No. DE-SC0001284).

References

[1] S.C. Singhal, Solid State Ionics 135 (2000) 305–313.
[2] A. Boudghene Stambouli, E. Traversa, Renew. Sustain. Energy Rev. 6 (2002) 433–455.
[3] H. Apfel, A. Rzepka, H. Tu, U. Stimming, J. Power Sources 154 (2006) 370–378.
[4] B. Kenney, K. Karan, Solid State Ionics 178 (2007) 297–306.
[5] M. Sase, J. Suzuki, K. Yashiro, T. Otake, A. Kaimai, T. Kawada, J. Mizusaki, H. Yugami, Solid State Ionics 177 (2006) 1961–1964.
[6] E. Koep, C.M. Jin, M. Haluska, R. Das, R. Narayan, K. Sandhage, R. Snyder, M.L. Liu, J. Power Sources 161 (2006) 250–255.
[7] E. Maguire, B. Gharbage, F.M.B. Marques, J.A. Labrincha, Solid State Ionics 127 (2000) 329–335.
[8] S.P. Jiang, J. Mater. Sci. 43 (2008) 6799–6833.
[9] D. Burnat, P. Ried, P. Holtappels, A. Heel, T. Graule, Fuel Cells 10 (2010) 156–165.
[10] M.H. Hung, M.V.M. Rao, D.S. Tsai, Mater. Chem. Phys. 101 (2007) 297–302.
[11] Q. Su, S. Cho, Z. Bi, A. Chen, H. Wang, Electrochim. Acta 56 (2011) 3969–3974.
[12] F. Tietz, H.P. Buchkremer, D. Stöver, Solid State Ionics 152–153 (2002) 373–381.
[13] S. Wang, J. Yoon, G. Kim, D.X. Huang, H. Wang, A.J. Jacobson, Chem. Mater. 22 (2010) 776–782.
[14] J. Yoon, S. Cho, J. Kim, J. Lee, Z. Bi, A. Serquis, X. Zhang, A. Manthiram, H. Wang, Adv. Funct. Mater. 19 (2009) 3868–3873.
[15] Z. Fan, F.B. Prinz, Nano Lett. 11 (2011) 2202–2205.
[16] S.B. Adler, Solid State Ionics 111 (1998) 125–134.
[17] J.H. Kim, A. Manthiram, J. Electrochem. Soc. 155 (2008) B385–B390.
[18] A. Bieberle-Hutter, H.L. Tuller, J. Electroceram. 16 (2006) 151–157.
[19] J. Yoon, R. Araujo, N. Grunbaum, L. Baque, A. Serquis, A. Caneiro, X.H. Zhang, H. Wang, Appl. Surf. Sci. 254 (2007) 266–269.
[20] A.J. Jacobson, Chem. Mater. 22 (2010) 660–674.
[21] L. Wang, R. Merkle, J. Maier, T. Acartürk, U. Starke, Appl. Phys. Lett. 94 (2009) 071908.
[22] G. Kim, S. Wang, A.J. Jacobson, L. Reimus, P. Brodersen, C.A. Mims, J. Mater. Chem. 17 (2007) 2500–2505.
[23] S. Biswas, T. Nithyanantham, N.T. Saraswathi, S. Bandopadhyay, J. Mater. Sci. 44 (2009) 778–785.
[24] I. Petrov, P.B. Barna, L. Hultman, J.E. Greene, J. Vac. Sci. Technol. A21 (2003) S117–S128.
[25] R. Messier, A.P. Giri, R.A. Roy, J. Vac. Sci. Technol. A 2 (1984) 500–503.
[26] M. Mogensen, N.M. Sammes, G.A. Tompsett, Solid State Ionics 129 (2000) 63–94.